A Satellite Perspective on the Interhemispheric Transport of Carbon Monoxide

Chenxia Cai[1,a*], Qinbin Li[1,2], Benjamin R. Lintner[2,3], Nathaniel J. Livesey[1]

[1] Jet Propulsion Laboratory, California Institute of Technology, Pasadena, California, USA

[2] Dept. of Atmospheric and Oceanic Sciences, University of California, Los Angeles, California, USA

[3]Institute of Geophysics and Planetary Physics, University of California, Los Angeles, California, USA

[a] Now at California Air Resources Board, Sacramento, California, USA

* Corresponding author: Chenxia Cai

Address: California Air Resources Board/PTSD, 1001 I street, Sacramento, CA, 95814

Email: ccai@arb.ca.gov

Phone: 916-322-1223, fax: 916-327-8524

Submit to Journal of Geophysical Research (December 2008)

Abstract: We investigate the spatiotemporal variability of interhemispheric transport (IHT) of pollution in the tropical upper troposphere as indicated by carbon monoxide (CO), by analyzing multi-year satellite observations of upper tropospheric CO from Aura-Microwave Limb Sounder (MLS) and Measurements of Pollution In The Troposphere (MOPITT) in conjunction with a global three-dimensional model (GEOS-Chem) simulation of atmospheric CO. Upper tropospheric CO fluxes computed with MLS and MOPITT observations exhibit strong longitudinal, seasonal and interannual variations that are consistent with GEOS-Chem results. The upper level IHT from Northern Hemisphere (NH) to Southern Hemisphere (SH) is strongest over the Indian Ocean in boreal summer and the Eastern Pacific in winter-spring. GEOS-Chem results of tagged CO tracers indicate that Asian fossil fuel and biofuel are the dominant sources to the strong IHT of CO over the Indian Ocean in summer, while the strong IHT of CO over the Eastern Pacific has large contributions from Asian fossil fuel and biomass burning from Asia and Africa. MOPITT CO vertical profiles show clear signatures of the vertical and subsequent cross-equatorial transport of CO over both regions. There is a significant correlation with a 5-day lag between precipitation rates, indicating the strength of the Indian Summer Monsoon (ISM), and MLS observed equatorial meridional CO gradients. This points to the impact of deep convection associated with the ISM on the IHT. Contrary to the conventional view that La Niña conditions favor IHT over the Eastern Pacific while El Niño conditions usually suppress it, our analysis shows that El Niño conditions could also enhance the “westerly ducts” and thus IHT over that region.

Introduction

Interhemispheric transport (IHT) is a key process affecting global redistribution of atmospheric air pollutants and greenhouses gases [*Newell et al.*, 1974; *Hartley and Black*, 1995; *Wang and Shallcross* 2000; *Staudt et al.*, 2001]. Improved understanding of IHT and its underlying mechanisms is necessary for both the quantification of sources and sinks of pollutants and the estimation of their potential to affect global climate, especially in light of projected anthropogenic climate change. IHT occurs predominantly in the tropical upper troposphere [*Prather et al.,* 1987; *Newell et al.,* 1974; *Plumb and Mahlman,* 1987 ; *Yamazaki and Chiba*, 1992]. Previous studies have indicated several mechanisms as potential generators of IHT. The occurrence of IHT through the upper troposphere has led to several hypotheses regarding the relationship of IHT to tropical convection. Using general circulation model (GCM)-derived estimates of CFC-11 fluxes, *Hartley and Black* [1995] implicated convective mixing followed by upper level divergence as a dominant IHT pathway. *Bowman and Cohen* [1997] noted the possible role of the Hadley circulation, its seasonal modulation, and associated chaotic advective dispersion as a source of IHT. *Lintner et al.* [2004] investigated the impacts of regional tropical convective intensification and location on 2-box model interhemispheric exchange times using a GCM and a reanalysis-driven chemical transport model (CTM). They identified the Indian Ocean as a "center of control" of IHT interannual variability during summer monsoon season.

Additionally, analyses of wave-mean flow interactions suggest that regions of time-mean westerlies in the tropical upper troposphere can support the propagation of transient waves between extratropics and tropics [*Arkin and Webster*, 1985; *Toms and*

Webster, 1996; *Webster and Holton*, 1982]. The occurrence of these so-called "westerly ducts" over the Eastern Pacific and tropical Atlantic [*Webster and Holton*, 1982; *Tomas and Webster*, 1994; *Waugh and Polvani*, 2000] has prompted consideration of their potential role in IHT. *Prinn et al.* [1992] proposed the cross-equatorial transport through "westerly ducts" to interpret the observed interannual variability of surface methylchloroform at Samoa (14°S, 171°E). *Staudt et al.* [2001] also argued for such a mechanism based on their modeling analysis of aircraft observations of upper tropospheric CO over the Eastern Pacific during the NASA Pacific Exploratory Mission in the tropical South Pacific Basin (PEM-Tropics B) in March-April 1999.

Two challenging aspects of IHT analyses are the substantial region-to-region and seasonal variations of IHT and the paucity of upper level measurements. Indeed, observation-based IHT studies have largely relied on sparse surface observations [*Prinn et al.*, 1992; *Denning et al.*, 1999; *Wang and Shallcross*, 2000] or aircraft campaigns with limited spatial as well as temporal sampling [*Staudt et al.*, 2001]. Satellite observations of tropical upper tropospheric chemical composition with continuous global coverage and consistent calibration, are thus very suited for IHT analysis. A byproduct of incomplete combustion with an atmospheric lifetime of ~2 months, tropospheric CO is a good tracer for pollution transport [*Liu et al.*, 2003; *Stohl et al.*, 2002]. Upper tropospheric CO retrievals from both the Aura Microwave Limb Sounder (MLS) [*Waters et al.*, 2006] and the Measurements of Pollution In The Troposphere (MOPITT) [*Drummond and Mand*, 1996] are thus ideal for a thorough examination of the variability of IHT [*Hartley and Black,* 1995; *Lintner et al.*, 2004]. More specifically, the multi-year, global coverage of the CO measurements from MLS and MOPITT provides a unique opportunity to

investigate the temporal and spatial characteristics of tropical upper tropospheric CO and its IHT. The present study is a first attempt to characterize IHT using multi-year CO observations from MLS and MOPITT.

In the present paper, we focus primarily on transport from the Northern Hemisphere (NH) to the Southern Hemisphere (SH). We use both MLS and MOPITT CO measurements to identify the tropical regions with the strongest southward cross-equatorial transport of CO in the upper troposphere. The temporal and spatial features, including vertical structures, of the satellite-observed CO concentrations for the entire tropics as well as selected regions are compared to results from the GEOS-Chem global 3D CTM simulations of CO [*Bey et al.*, 2001]. The GEOS-Chem simulations include CO tracers for total direct emissions as well as different source regions (e.g, Asia, North America, Europe, Africa, South America) and source types (e.g., fossil fuel, biomass burning, biofuel); the 'tagged' CO tracers are used to diagnose contributions of distinct source regions or types to tropical upper tropospheric CO distributions and IHT. Finally, the modulating effects of the Indian Summer Monsoon (ISM) and El Niño/Southern Oscillation (ENSO) on tropical upper tropospheric CO distributions and IHT are examined.

2. Observations and Model Simulations

2.1 Aura-MLS CO

The MLS on Aura satellite launched in July 2004 observes thermal microwave limb emission from many molecules including CO in Earth's upper troposphere, stratosphere and mesosphere. MLS CO in the upper troposphere has a precision of ~15-

40 ppbv with horizontal and vertical resolutions of ~500-600 km and 4 km, respectively. MLS CO retrievals in the upper troposphere are generally not contaminated by the presence of clouds. Only the CO retrievals for the layers above 215 hPa are suggested for scientific uses for the current data release. While there is evidence of about a factor of two high bias in MLS CO at 215 hPa, no bias is seen at 147 hPa. MLS applies *a priori* data to constrain the retrieval results as commonly used in remote sensing technique [*Rodgers*, 2000]. To minimize the influence of *a priori* data, only the data with retrieval uncertainty less than 50% of the *a priori* uncertainty are suggested for scientific studies. More detailed descriptions of the CO retrieval are presented in *Livesey et al.* [2008]. We use in the present study MLS CO (v1.5) concentrations at 147 hPa, where MLS has good sensitivity for CO, from September 2004-August 2006, averaged onto 4° (latitude) × 8° (longitude) grids. MLS CO data have been previously used to study CO enhancement and transport in the upper troposphere and low stratosphere (UTLS) [*Li et al.*, 2005; *Park et al.*, 2007] and the impacts of convection and emissions on UTLS CO [*Fu et al.*, 2005; *Jiang et al.*, 2007].

2.2 MOPITT CO

MOPITT is a nadir-viewing infrared correlation radiometer that was launched aboard the EOS Terra satellite in 1999 and monitors the global distribution of CO from a polar-orbiting platform [*Deeter et al.*, 2003, 2004]. It provides nearly global coverage in 3 days with a horizontal resolution of 22 km^2. CO concentrations are reported on 7 vertical levels and as a column for cloud-free scenes. Both the CO concentrations and column have a 10% precision [*Deeter et al.,* 2003]. The MOPITT data used here (version

3) are for January 2000 - January 2007. Only the data with a percentage of *a priori* contribution less than 50% are used in this study. The CO data used here are averaged onto 1° × 1° grids. It has been shown that MOPITT can independently retrieve mid- and upper-tropospheric CO [*Deeter et al.,* 2004] and detect the vertical transport of tropospheric CO [*Kar et al.*, 2004]. MOPITT data have also been used to study the trans-pacific transport of CO [*Heald et al.*, 2003] and the impacts of ENSO on tropospheric CO [*Edwards et al.*, 2006].

2.3 NCEP Winds and GPCP Precipitation

We make use of wind and precipitation data to relate the spatiotemporal features of CO to tropospheric circulation and convection. Specifically, wind vectors are used to indicate large-scale circulations. The meridional winds are used in computing the meridional CO fluxes across the equator. Precipitation rates are used as a proxy for the location of the Intertropical Convergence Zone (ITCZ), generally considered a barrier for low-level IHT [*Waliser and Gautier*, 1993; *Staudt et al*., 2002]. Additionally, precipitation data over the Indian Ocean during summer are used to indicate the strength of the ISM.

The wind fields are from the NCAR/NCEP reanalysis [*Kalnay et al.*, 1996], available at http://www.cdc.noaa.gov/ at a horizontal resolution of 2.5° × 2.5°. Precipitation data are from the Global Precipitation Climatology Project (GPCP) [*Huffman et al.*, 2001; *Alder et al.*, 2003], available at http://precip.gsfc.nasa.gov/index.html. The precipitation data have a spatial resolution of 2.5° × 2.5° and 1° × 1° for monthly and daily means, respectively.

2.4 GEOS-Chem Model Description and Simulations

The GEOS-Chem model is a global 3-D model of atmospheric composition driven by assimilated meteorological data from the Goddard Earth Observing System (GEOS-4) of the NASA Global Modeling Assimilation Office (GMAO). The GEOS-4 meteorological data are available at 1° × 1° horizontal resolution and 55 hybrid eta levels in the vertical extending from the surface to 0.01 hPa (~70 km). The physics in the GEOS-4 reanalysis system are adopted from the NCAR Community Climate Model, Version 3 (CCM3) and Whole Atmosphere Community Climate Model (WACCM) with modifications to make it suitable for data assimilation [*Bloom et al*., 2005]. The deep convection scheme is based on *Zhang and McFarlane* [1995], and the shallow convection treatment follows *Hack* [1994]. Tracer advection is computed every 15 minutes with a flux-form semi-Lagrangian method [*Lin and Rood*, 1996]. Tracer moist convection is computed using the GEOS convective, entrainment, and detrainment mass fluxes described by *Allen et al.* [1996a, 1996b].

To identify source regions and types contributing to IHT of CO, we transport separately in the model a suite of CO tracers, i.e., "tagging" emissions from different source regions and types, a technique that has been used previously in a number of GEOS-Chem applications [*Liu et al*, 2001; *Sinha et al.*, 2004, *Staudt et al.*, 2001]. We present here global simulations of CO conducted at 2° × 2.5° resolution (i.e., by degrading the meteorological data from 1° × 1° to 2° × 2.5° for computational consideration) for 2005 using GEOS-Chem v7-04-10. CO sources in the GEOS-Chem model include fossil fuel and biofuel combustion, biomass burning emissions, and

chemical production from atmospheric oxidation of methane, isoprene, and other volatile organic compounds (VOCs). Biomass burning emissions are from the Global Fire Emissions Database Version 2 (GFED V2) [*Randerson et al.,* 2007] with a monthly temporal resolution. Biofuel emissions are from *Yevich and Logan* [2003]. Anthropogenic emissions are based on *Benkovitz, et al.* [1996]. Archived monthly mean OH concentrations from a standard GEOS-Chem full-chemistry simulation are used to calculate the chemical production and loss of CO.

3. Monthly Cross-Equatorial CO fluxes

We consider first the longitudinal variation of IHT during different seasons by examining meridional CO mass fluxes in the tropical upper troposphere. For our analysis we divide the tropics longitudinally into sub-domains. Africa, the Indian Ocean, the Eastern Pacific, South America, and the Atlantic, defined here as 10°-40°E, 60°-100°E, 140°-100°W, 75°-45°W and 40°-10°W, respectively, following *Waliser and Gautier* [1993]. We examine here CO fluxes computed from the MOPITT and MLS CO observations and GEOS-Chem results. The fluxes are estimated by multiplying monthly CO concentrations by NCEP reanalysis meridional wind velocities at either 150 hPa (MOPITT) or 147 hPa (MLS and GEOS-Chem). We focus our analysis on the CO fluxes averaged over the tropical latitudinal band of 16°S-16°N as a way to mitigate the effect of ITCZ migration on our conclusions [*Hartley and Black*, 1995].

Figures 1a,b,c show CO fluxes for September 2004-September 2006 from MLS, January-December 2005 from GEOS-Chem, and January 2000-January 2007 from MOPITT, respectively. CO fluxes from MLS and GEOS-Chem show consistent seasonal

and longitudinal variability. Strong southward CO fluxes are seen over the Eastern Pacific and the Atlantic during boreal winter and early spring. For boreal summer through early fall (June-October), southward CO fluxes dominate most of the equatorial region, particularly over 60°E-140°E (the Indian Ocean and western Pacific) with maximum southward CO fluxes over the Indian Ocean in June and July. At the same time a secondary peak of southward CO fluxes is seen over western South America. There are strong northward CO fluxes over much of the tropics from January to May with the largest northward fluxes occuring over 60°W-40°W (South America), 0°-30°E (Africa). Model simulations indicate that a large part of these northward CO fluxes can be attributed to biomass burning emissions from these regions.

While there is a general consistency between the patterns of CO fluxes from MLS and GEOS-Chem, the magnitude of GEOS-Chem CO fluxes are typically smaller than the MLS CO fluxes. For instance, the maximum southward CO flux from MLS over the Indian Ocean during June-July 2005 is over 1.8×10^{-7} kg m^{-2} s^{-1}, while the maximum from GEOS-Chem is $1.2\text{-}1.5\times10^{-9}$ kg m^{-2} s^{-1}. The difference however does not affect our analysis here since our focus is on the spatiotemporal distribution and variability of cross-equatorial CO flux. Clearly more attention needs to be on the absolute CO values for a closer look at the relative importance of different processes influencing IHT and for diagnosing any deficiencies in the model. That is beyond the scope of the present study.

The MOPITT CO fluxes (Figure 1c) exhibit seasonal variability and longitudinal structure that are broadly consistent with those from both MLS and GEOS-Chem. Additionally, significant interannual variability of upper tropospheric CO fluxes is obvious, as evident in the southward CO fluxes over the Indian Ocean in summer. Over

the Eastern Pacific, the southward CO fluxes during the winter of 2004/2005 are particularly strong compared with other winters. Such strong southward CO fluxes can also be seen over the Atlantic during the same time period. Eastern Pacific region circulation experiences considerable interannual variability associated with the ENSO, the impact on tracer distributions and IHT will be discussed in section 7. Given the strong seasonal cross-equatorial CO fluxes over the Indian Ocean and Eastern Pacific, we take a closer look at these locations in the following sections.

4. IHT of CO During Winter and Summer

In this section we examine the IHT of CO in boreal winter and summer over the tropical Eastern Pacific and Indian Ocean. More specifically, we examine monthly mean tropical upper tropospheric CO concentrations and fluxes from January and July 2005 in relation to upper-level circulations. We limit our analysis on the monthly mean meridional transport only in this study and leave a more detailed analysis of both mean and transient meridional transport for a future study. It is worth pointing out that the occurrence of large mean southward velocities over the Eastern Pacific during boreal winter is dynamically linked to the presence of the mean westerlies [*Tomas and Holton*, 1994].

4.1 January 2005

Figure 2a shows 147 hPa CO for January 2005 from MLS and GEOS-Chem. Our focus here is on the tropics. The spatial structures of MLS and GEOS-Chem CO show broad agreement. The enhanced CO levels over Africa, South Asia, and South America

are seen in both the observations and model results. Peak CO concentrations are generally higher in the MLS observations than GEOS-Chem model results. Over the tropical Eastern Pacific where strong southward meridional winds and CO fluxes are seen (see Figure 1 and discussions in section 3), the CO concentrations are relatively low compared to other tropical regions. MOPITT data, not shown here, also show similar spatial distributions of CO at 150 hPa.

Previous studies have shown that the long-range transport of Asian CO emissions contributes significantly to CO over the Eastern Pacific [*Liu et al.*, 2003; *Staudt et al.*, 2002; *Yienger et al*., 2000]. To better understand the source contributions to IHT of CO, we show in Figure 3a the spatial distribution of GEOS-Chem simulated monthly mean fluxes of CO emitted from Asian fossil fuel combustion. NCEP winds and GPCP precipitation rates are also shown with the latter indicating the ITCZ zone. There are strong eastward Asian fossil fuel CO fluxes at 20-30°N. Relatively strong southeastward Asian fossil fuel CO fluxes are also seen over the tropical Eastern Pacific, extending all the way south to 10°S. A similar but weaker southeastward Asian fossil fuel CO fluxes is evident over the Atlantic. Over the tropical western Pacific, there are strong northward Asian fossil fuel CO fluxes.

A modeling study by *Staudt et al*. [2001] showed the existence of southeastward Asian CO fluxes in the upper troposphere over the tropical Eastern Pacific during the PEM-Tropics aircraft campaign (March-April 1999). Our model results indicate that, for 2005 at least, the southeastward Asian fossil fuel CO fluxes are stronger in January-February than March-April (not shown). The strong southeastward Asian fossil fuel CO fluxes over the tropical Eastern Pacific and Atlantic occur in regions of mean westerly

flow, consistent with the notion of westerly ducts and the associated IHT [*Staudt et al.*, 2001].

4.2 July 2005

One of the prominent features of the July wind fields at 147 hPa is the upper tropospheric anticyclone over South Asia (Figure 2b). The anticyclone is associated with the ISM circulation, one of the most energetic components of the Earth's climate system [*Wang et al.*, 2001; *Krishnamurti and Bhalme*, 1976]. Collocated with the upper level anticyclone are prominent CO maxima in both the MLS observations and GEOS-Chem model results (Figure 2b). Previous studies [*Li et al.*, 2005, *Jiang et al.*, 2007] have suggested that convections associated with the ISM circulation lift pollutants emitted from northern Indian and southwest China into to the upper troposphere and can be trapped by the upper level anticyclone. The strong northeasterly wind on the southern flank of the anticyclone provides a transport pathway for south Asian CO to over the northern Indian Ocean and further to the SH (Figure 2b). Figure 3b shows GEOS-Chem simulated monthly mean Asian fossil fuel CO fluxes at 147 hPa for July 2005. Also shown are NCEP winds and GPCP precipitation rates. Indeed, our model results clearly show the southwestward Asian CO fluxes across the equator and the ITCZ zone which indicates the strong IHT occurring over the ISM region.

5. Temporal Variations and Source Attributions of Upper Tropospheric CO

We now investigate in more detail the temporal variations of IHT of CO over the tropical Eastern Pacific and Indian Ocean. Again, we focus our analysis on tropical upper

tropospheric CO from 2005. In this section we will expand from the previous section our analysis on the source regions and types contributing to the IHT of CO.

5.1 Indian Ocean

Figures 4a shows time-latitude plots of 5-day average CO concentrations from MLS, MOPITT, and GEOS-Chem for the Indian Ocean. GPCP precipitation rates are also shown as an indicator of the location of the ITCZ zone. Over the Indian Ocean, the intensity and location of ITCZ exhibit strong seasonal dependencies. During boreal spring, the ITCZ generally lies between 20°S to 5°N. During boreal summer, there is a broad ITCZ band extending from about 15°S to 25°N. The ITCZ is located between mostly 15°S to 15°N during boreal fall and winter. The northward expansion of ITCZ reflects the intensification of convection associated with the ISM.

The annual cycles of upper tropospheric CO concentrations from MLS, MOPITT and model simulation show similar patterns over the Indian Ocean. The upper tropospheric CO concentrations exhibit strong meridional gradients throughout the year in all three datasets. Notably, there are several periods of significant CO enhancements. During January 1-10, CO concentrations exceeding 100 ppbv at 5°N-20°N were observed by MLS and MOPITT. GEOS-Chem captures this enhancement albeit with lower CO concentrations. CO enhancements between 5°S-20°N during March appear in all three datasets. GEOS-Chem shows enhanced CO also in April, which is not present in MLS nor in MOPITT. During summer, both the observations and model results show enhanced CO to the north of the equator, consistent with northward expansion of the ITCZ. MLS

and MOPITT data show enhanced CO during June-October. GEOS-Chem model results, however, show enhanced CO starting in May through October.

Figures 5a shows time-latitude plots of GEOS-Chem simulated anthropogenic and biomass burning CO tracers in the tropical upper troposphere over the Indian Ocean. Our model results show the CO enhancement in early January (Figure 4a) is dominated by Asian fossil fuel emissions and to a less degree Asian biofuel emissions. Asian biofuel and fossil fuel emissions are also the dominating sources for the enhanced CO during June-October. Biomass burning emissions from Southeast Asia and northern Africa are the largest contributors to the CO enhancements during February-March. The enhanced CO in April-June (Figure 4a) is largely from Southeast Asia biomass burning emissions. The enhanced CO in the southern tropics in September-October is primarily from Australian biomass burning emissions.

5.2 Eastern Pacific

Over the Eastern Pacific, the MLS, MOPITT and GEOS-Chem CO data also show consistent temporal fluctuations (Figure 4b). Compared to the Indian Ocean, CO concentrations over the Eastern Pacific are generally lower throughout the year, but some periods of enhanced CO are evident. Relatively higher CO concentrations are observed in January and March-May over the northern tropics by MLS and MOPITT, with slightly different latitudes of maximum CO between the two data sets. For example, the January CO maximum is located at about 10°N from MLS and at 20°N from MOPITT. CO concentrations for January are much lower in GEOS-Chem simulation. The model shows enhanced CO during March-May, consistent with the observations. The model results

also show enhancements at 5°-15°N during days 201-205 and days 226-235, but enhancements during these time periods are not as strong nor obvious in the MLS and MOPITT data. Enhanced CO concentrations between 20°S-10°S are present in MLS and MOPITT data during October-November, which are not apparent in the model results.

Figure 5b shows that the enhanced CO in the upper troposphere over the tropical Eastern Pacific during boreal winter (Figure 4b) is dominated by Asian fossil fuel and to a lesser degree biofuel emissions. African and Asian biomass burning emissions are the two largest sources contributing to the CO enhancements in February-April and April-June, respectively. They are also the strongest contributions to the cross-equatorial transport of CO during March-June over the tropical Eastern Pacific. During boreal summer, North American fossil fuel emissions have the largest contribution to CO over the northern tropical Eastern Pacific. Figure 5b also indicates that the high CO concentrations prevailing over the southern tropical Eastern Pacific during October-November are predominantly from South American biomass burning emissions.

6. Vertical Distribution of CO

Previous modeling studies have suggested that IHT occurs predominantly in the upper troposphere [*Prather et al.,* 1987; *Newell et al.,* 1974; *Plumb and Mahlman,* 1987; *Yamazaki and Chiba,* 1992, *Staudt et al.*, 2002]. For example, the modeling study by *Prather et al.* [1987] showed significant IHT of CFCs between 100-400 hPa. The modeling study by *Staudt et al.* [2001] also showed strong meridional CO fluxes from northern hemisphere sources to 20°S at altitudes of 11-12 km (~200 hPa) over the Eastern Pacific in spring. In this section we examine the detailed vertical structure of the IHT of

CO, considering that mean CO flux estimates for a given pressure level (as in Section 4) may be largely offset or compensated by transport of the opposite sign at other pressure levels. We examine here GEOS-Chem simulated and MOPITT observed vertical distributions of tropical tropospheric CO in relation to circulation. Our analysis again focuses on the tropical Eastern Pacific in January and Indian Ocean in July 2005.

Height-latitude distributions of GEOS-Chem monthly CO from northern hemisphere anthropogenic sources averaged over the Eastern Pacific for January 2005 and the Indian Ocean for July 2005 are presented in Figures 6a and 6b, respectively. Over the Eastern Pacific in January, the strongest southward meridional winds (vectors) are at 300-100 hPa, and low-level northward flow is also evident (Figure 6a). This baroclinic wind structure reflects low-level inflow from the northern hemisphere into the ITCZ (at ~10°N) followed by upper-level outflow into the southern hemisphere. The strongest low level meridional CO gradients occur in the vicinity of the ITCZ and the orientation of CO isolines in low latitudes of the SH, with higher CO aloft, is indicative of upper level IHT. Similarly for the Indian Ocean during July 2005, northern hemispheric anthropogenic CO is transported southward predominantly in the upper troposphere at 250-100 hPa, where strongest southward meridional winds prevail. Some hint of the vertical transport of elevated CO from upper troposphere to mid-troposphere in the subsiding branch of the monsoon region "local Hadley" circulation (~20-30°S) is also evident.

Analysis of the averaging kernels of CO retrieved from MOPITT satellite measurements suggests that, even though the averaging kernels are not sharply defined, CO vertical profiles from MOPITT retrievals can provide sufficient information to discriminate the middle and upper troposphere [*Emmons et al.*, 2004, *Kar et al.*, 2004;

Deeter et al., 2004; see the latter for typical average kernels of MOPITT CO retrievals for tropical oceanic regions]. We computed height-latitude cross-section of monthly MOPITT CO using daytime retrievals only since the degree of freedom (DOF), a measure of the independent pieces of information provided by the retrieval, falls sharply at night [*Kar et al.*, 2004]

For the MOPITT-derived cross-section of CO profiles over the Eastern Pacific in January (Figure 7a), strong IHT is clearly seen at 500-150 hPa in the upper troposphere. Similar to the results in *Kar et al.* [2004], the broad layer of IHT reflects the smoothing influence of the MOPITT retrievals with broad averaging kernels. For the Indian Ocean, in July (Figure 7b) the effect of southward transport of CO in the upper troposphere is also clearly evident. The CO transported across the equator into the SH is subsequently mixed with biomass burning emissions from Australia and outflow from Africa [*Edwards et al.,* 2006]. Note that in Figure 6b, only GEOS-Chem simulated CO from NH anthropogenic sources are shown hence no enhanced CO in the lower and middle troposphere in the southern hemisphere, while in Figure 7b total CO from MOPITT is shown. The strong resemblance of the vertical distributions of CO from GEOS-Chem and MOPITT as shown in Figures 6 and 7 indicates that the GEOS-Chem simulation and MOPITT observations are reflecting similar IHT mechanisms.

7. Impact of large-scale circulation on IHT

7.1 Indian Summer Monsoon

We have shown in previous sections that the southward upper tropospheric CO fluxes over the Indian Ocean are influenced by the ISM circulation. We now consider

whether changes in the intensity of the ISM are reflected in the CO data. In particular, the strengthening of the ISM could conceivably lead to intensified cross-equatorial flow as well as the enhanced upper tropospheric CO through the uplift of CO from surface emissions via stronger deep convection, both of which may favor IHT enhancement.

Metrics for monsoon intensity are typically based on either precipitation or dynamical quantities [*Parthasarathy et al.*, 1992; *Parthasarathy et al.*, 1995; *Wang et al.* 2001]. Here we use a precipitation-based index of 5-day means of GPCP precipitation averaged over 60°E-100°E and 16°N-16°S. Additionally, the dynamical index of *Wang et al*. [2001], which is defined as the difference of 850 hPa zonal winds between regional average of 5°-15°N, 40°-80°E and of 20°-30°N, 70°-90°E is also considered. For a measure of the IHT, we use the difference of upper tropospheric CO for the Indian Ocean between 16°N and 16°S, this choice is analogous to a notional 2-box model view in which the steepness of the interhemispheric gradient is related to the relative amount of mixing between the two hemispheres, i.e., a steeper (weaker) gradient indicates less (more) IHT.

Regression analyses of 5-day means of precipitation versus either the MOPITT or MLS CO gradients over Indian Ocean during 2005 summer monsoon months (JJAS) are shown in Figure 8. The 5-day means of MOPITT CO gradients are relatively flat (upper panel, Figure 8). It is possible that MOPITT could underestimate abundances at this level in enhanced conditions due to its broader resolution. The MLS values, which generally are not contaminated by the presence of clouds and more sensitive at 147 hPa level, display much stronger high-frequency variability. The scatter-plots in Figure 8 (upper panel) show only weak anti-correlations ($R^2 = 0.1$) between precipitation versus MOPITT

CO gradients and precipitation versus MLS CO gradients. Further regression analysis using the CO gradients lagging precipitation by 5 days (bottom panel, Figure 8) yields a much stronger anti-correlation (R^2 = 0.5) for MLS but little change for MOPITT. Increasing the time lag to 10 days gives $R^2 < 0.1$. The regression between MLS CO and the precipitation hints at a relationship between intensified monsoon conditions and weakened upper tropospheric CO gradients, with the latter associated with enhanced IHT. The stronger anti-correlation with a 5-day time lag suggests that the likely time interval for convection to have a direct impact on IHT is on the order of a few days. Similar regression analyses are performed using the *Wang et al.* [2001] index as the monsoon index. The results, however, show general weakness of the anti-correlations (R^2 = 0.1) between the *Wang et al.* [2001] index and CO gradient from both MOPITT and MLS with and without a 5-day lag. Of course, the impact of convection on IHT is a very complicated process, and perhaps the monsoon indices used here do not fully capture those aspects of monsoon intensity change that are relevant to IHT. Also, the CO gradient may be affected by other sources of variability.

7.2 ENSO effect on IHT over Eastern Pacific

Circulation over the Eastern Pacific exhibits considerable interannual variability associated with ENSO. These changes are likely to impact on pollution transport and the IHT. For example, the westerly duct and associated IHT may be intensified under La Niña conditions, when upper level westerlies are strengthened, and weakened under El Niño periods, when upper level westerlies are suppressed [*Tomas and Webster*, 1994, *Waugh and Polvani*, 2000]. However, our examination of the MOPITT CO, winds, and

sea surface temperature (SST) data for 2000-2006 suggests a more complex relationship between ENSO and the IHT of CO that hinges on the precise structure of anomalous ENSO forcing and its relationship to the mean state. Figure 3a shows that there are strong southward cross-equatorial CO fluxes in the tropical upper troposphere over the Eastern Pacific during the winter of 2004-2005, a moderate El Niño winter. The southward CO fluxes are accompanied by strong northward CO fluxes over the Central Pacific. Additionally, there are strong southward CO fluxes in the tropical upper troposphere over the Atlantic during the same period.

Figure 9 shows 150 hPa NCAR/NCEP wind anomalies for January-February 2005 with respect to the 1968-1996 long-term mean. The color contours in this figure show the anomalies in NOAA extended reconstructed sea surface temperature (SST) for the same time period with respect to the 1971-2000 long-term mean. The positive westerly anomaly indicates that the strengthening of westerly duct during these two months is associated with stronger northerly meridional wind. The enhanced northwesterterlies over the Eastern Pacific can be explained by the anomalous SST forcing through a Gill [1980]-type model of the tropospheric response to an imposed heating anomaly. In particular, to the east of the heating anomaly, anomalous upper level westerlies develop in response to upper level divergence associated with enhanced convection over the anomalous SST region. From Figure 9, it is clear that the positive SST anomaly was located in the Central Pacific rather than the Eastern Pacific, so that the warm event conditions at this time were associated with a stronger, rather than weaker, westerly duct.

8. Summary and Discussions

We have analyzed multi-year satellite CO observations from MLS and MOPITT as well as the CO simulations using GEOS-Chem model simulation to show the spatiotemporal variability of upper tropospheric CO and its IHT. The cross-equatorial CO fluxes derived from MLS and MOPITT observations and GEOS-Chem model results in conjunction with NCEP reanalysis wind fields suggest that upper tropospheric CO IHT exhibits strong temporal variability on timescales ranging from synopitic to interannual. Strongest southward CO fluxes are found over the Indian Ocean in boreal summer and the Eastern Pacific in boreal winter to spring. While the observations and simulations show broadly consistent patterns of IHT variability, difference in meridional CO fluxes magnitudes derived from observations and the simulations are associated with systematic biases between the model and the observations. GEOS-Chem 'Tagged-CO' simulations show that the largest portion of the CO IHT over the Indian Ocean in boreal summer (June to August) is from Asian biofuel and fossil fuel emissions. The vertical distribution of modeled CO tracers shows CO associated with NH anthropogenic sources entered SH predominantly via the layers between 250 hPa to 100 hPa over Indian Ocean during boreal summer. Over the Eastern Pacific in boreal winter, Asian fossil fuel is the major contributor to the CO IHT while in boreal spring biomass burning from Asian and northern Africa are the major contributors. The CO from NH anthropogenic sources are transported to SH at the level ranging from 300 hPa to 100 hPa over Eastern Pacific during boreal winter. Vertical profiles retrieved from MOPITT have been shown to be capable of detecting the IHT in upper troposphere over Indian Ocean and Eastern Pacific during boreal summer and winter respectively. The possible effect on IHT over Indian

Ocean from the changes in the intensity of the ISM was investigated by conducting regression analysis of the strength of ISM (indicated by precipitation) and the CO north-south gradient with a strong anti-correlation evident between 5-day averages of precipitation and MLS observed CO gradients between 16ºN and 16ºS at 147 hPa at a 5-day lag. Such anti-correlation is not clear from MOPITT CO or if a dynamical index is used as the indicator for the strength of ISM. Although previous studies have shown that La Niña conditions favor IHT over the Eastern Pacific while El Niño conditions usually suppress it, our analysis shows enhanced north-westerlies associated with stronger southward IHT of CO over Eastern Pacific during a moderate El Niño winter in which the SST anomaly occurred within the central Pacific.

Acknowledgment:

This work was performed at the Jet Propulsion Laboratory (JPL), California Institute of Technology, under contract with NASA. We thank Duane Waliser and Baijun Tian for helpful discussions. C. Cai was in part supported by the NASA Atmospheric Composition Modeling and Analysis Program (ACMAP) and the MLS project. Q. Li was supported by ACMAP. N. Livesey was supported by the MLS project. The GEOS-Chem model is managed at Harvard University with support from NASA ACMAP.

Reference:

Adler, R.F., G.J. Huffman, A. Chang, R. Ferraro, P. Xie, J. Janowiak, B. Rudolf, U. Schneider, S. Curtis, D. Bolvin, A. Gruber, J. Susskind, P. Arkin, and E. Nelkin (2003): The Version 2 Global Precipitation Climatology Project (GPCP) Monthly Precipitation Analysis (1979-Present). J. Hydrometeor., 4, 1147-1167.

Allen, D. J., R. B. Rood, A. M. Thompson, and R. D. Hidson (1996a), Three-dimensional ^{222}Rn calculations using assimilated data and a convective mixing algorithm, *J. Geophys. Res.*, *101*, 6871-6881.

Allen, D. J., *et al*. (1996b), Transport induced interannual variability of carbon monoxide using a chemistry and transport model, *J. Geophys. Res.*, *101*, 28655-28670.

Arkin, P. A. and P. J. Webster (1985), Annual and interannual variability of tropical-extratropical interaction: An empirical study, Mon. Weath. Rev., 113, 1510-1523.

Benkovitz, C. M., et al. (1996), Global gridded inventories of anthropogenic emissions for sulfur and nitrogen, J. Geophys. Res., 101 (D22), 29,239 -29,253.

Bey, I., d. J. Jacob, R. M. Yantosca, J. A. Logan, B. D. Field, a. M. Fiore, Q. Li, H. Y. Liu, L. J. Mickley, and M. G. Schultz (2001), Global modeling of tropospheric chemistry with assimilated meteorology: Model description and evaluation, J. Geophys. Res., 106, 23,073-23,089.

Bloom, S., *et al*. (2005), The Goddard Earth Observation System Data Assimilation System, GEOS DAS Version 4.0.3: Documentation and Validation, NASA TM-2005-104606, *26*, 166pp.

Bowman, K. P., and P. J. Cohen (1997), Interhemispheric exchange by seasonal modulation of the Hadley circulation, J. Atmos. Sci., 54, 2045-2059.

Denning, A. S., et al. (1999), Three-dimensional transport and concentration of SF6-A model intercomparison study (TransCom 2), Tellus, Ser. B, 51, 266-297.

Deeter , M. N., et al. (2003), Operational carbon monoxide retrieval algorithm and selected results for the MOPITT instrument, J. Geophys. Res., 108(D14), 4399, doi:10.1029/2002JD003186.

Drummond, J. R and G. S. Mand (1996), The measurements of pollution in the troposphere (MOPITT) instrument: Overall performance and calibration requirements. *J. Atmos. Ocean. Technol.*, 13:314-320.

Edwards, D. P., et al. (2006), Satellite-observed pollution from Southern Hemisphere biomass burning, J. Geophys. Res., 111, D14321, doi:10.1029/2005JD006655.

Gill, A. E. (1980), Some simple solutions for heat-induced circulation of the tropical atmospheres, quart. J. Roy. Meteor. Soc., 106, 447-462

Gille, R. N. Hoffman, and T. Nehrkorn (2004), Comparative inverse analysis of satellite (MOPITT) and aircraft (TRACE-P) observations to estimate Asian sources of carbon monoxide, *J. Geophys. Res.*, *109*, D23306, doi:10.1029/2004JD005185.

Hartley, D. E., and R. X. Black (1995), Mechanistic analysis of interhemispheric transport, *Geophys. Res. Lett.*, 22, 2945-2948.

Heald, C. L., D. J. Jacob, D. B. A. Jones, P. I. Palmer, J. A. Logan, D. G. Streets, G. W. Sachse, J. C. Gille, R. N. Hoffman, and T. Nehrkorn (2004), Comparative inverse analysis of satellite (MOPITT) and aircraft (TRACE-P) observations to estimate Asian sources of carbon monoxide, *J. Geophys. Res.*, *109*, D23306, doi:10.1029/2004JD005185.

Huffman, G.J., R.F. Adler, M. Morrissey, D.T. Bolvin, S. Curtis, R. Joyce, B McGavock, and J. Susskind (2001): Global Precipitation at One-Degree Daily Resolution from Multi-Satellite Observations. J. Hydrometeor., 2, 36-50.

Jiang, J.H., N.J. Livesey, H. Su, L. Neary, J.C. McConnell, and N.A. Richards (2007), Connecting surface emissions, convective uplifting, and long-range transport of carbon monoxide in the upper-troposphere: New observations from the Aura Microwave Limb Sounder, *Geophys. Res. Lett. 34*, L18812, doi:10.1029/2007GL030638.

Kalnay et al. (1996), The NCEP/NCAR 40-year reanalysis project, Bull. Amer. Meteor. Soc., 77, 437-470.

Kar, J., et al. (2004), Evidence of vertical transport of carbon monoxide from Measurements of Pollution in the Troposphere (MOPITT), *Geophys. Res. Lett.*, *31*, L23105, doi:10.1029/2004GL021128.

Li, Q., et al. (2005), Convective outflow of South Asian pollution: A global CTM simulation compared with EOS MLS observations, Geophys. Res. Lett., 32, L14826, doi:10.1029/2005GL022762.

Lin, S. J., and R. B. Rood (1996), Multidimensional flux form semi-Lagrangian transport schemes, *Mon. Weather Rev.*, *124*, 2046-2070.

Lintner, B. R., A. B. Gilliland and I. Y. Fung (2004), Mechanisms of concection-induced modulation of passive tracer interhemispheric transport interannual variability, J. Geophys. Res., 109, D13102, doi:10.1029/2003JD004306.

Liu, H., D. J. Jacob, I. Bey, R. M. Yantosca, B. N. Duncan, and G. W. Sachse (2003), Transport pathways for Asian pollution outflow over the Pacific: Interannual and

seasonal variations, J. Geophys. Res., 108(D20), 8786, doi:10.1029/2002JD003102.

Livesey, N.J., et al., Validation of Aura Microwave Limb Sounder O3 and CO observations in the upper troposphere and lower stratosphere," *J. Geophys. Res.*, in press.

Newell, R. E., G. J. Boer Jr., and J. W. Kidson (1974), And estimate of the interhemispheric transfer of carbon monoxide from tropical general circulation data, Tellus, 26,103-107.

Park, M., W.J. Randel, A. Gettleman, S.T. Massie, and J.H. Jiang (2007), Transport above the Asian summer monsoon anticyclone inferred from Aura MLS tracers, *J. Geophys. Res. 112*, D16309, doi:10.1029/2006JD008294.

Plumb R. A., and J. D. Mahlman (1987): The zonally averaged transport characteristics of the GFDL general circulation/transport model. *J. Atmos. Sci.*, **44**, 298–327.

Prather, M., M. McElroy, S. Wofsy, G. Russell, and D. Rind (1987), Chemistry of the global troposphere-fluorocarbons as tracers of air motion, J. Geophysc. Res., 92,6579-6613.

Prinn. R., et al. (1992), Global average concentration and trend for hydroxyl radicals deduced from ALE/GAGE trichloroethane (methyl chloroform) data for 1978-1990, J. Geophys. Res., 97, 2445-2461.

Rodgers, C. D (2000), Inverse methods for atmospheric sounding: Theory and practice, World Sci., Hackensack, N.J.

Seinfeld. J. H. and S. N. Pandis (1998), Atmospheric Chemistry and physics: From air pollution to climate change, John wiley & Sons, Inc.

Sinha, Pl, L. Jaegle, P. V. Hobbs, and Q. Liang (2004), Transport of biomass burning

emissions from southern Africa, J. Geophys. Res., 109, D20204, doi:10.1029/2004JD005044.

Staudt, A. C., D. J. Jacob, J. A. Logan, D. Bachiochi, T. N. Krishnamurti, and G. W. Sachse (2001), Continental sources, transoceanic transport, and interhemispheric exchange of carbon monoxide over the Pacific, *J. Geophys. Res.*, 106, 32,571-32,590,

Stohl, A., S. Eckhardt, C. Forster, P. James, and N. Spichtinger (2002), On the pathways and timescales of intercontinental air pollution transport, J. Geophys. Res., 107 (D23), 4684, doi:10.1029/2001JD001396.

Tomas, R. W., and P. J. Webster (1994), Horizontal and vertical structure of cross-equatorial wave propagation, J. Atmos. Sci., 51, 1417-1430.

Wang, K. Y., and D. E. Shallcross (2000), A modeling study of tropospheric distributions of the trace gases CFC13 and CH3CC13 in the 1980s, *Ann. Geophys.*, 18, 972-986.

Waliser and Gautier (1993), A Satellite-derived climatology of the ITCZ, *J. Clim.*, vol.6, 2162-2174.

Waugh, D. W., and L. M. Polvani (2000), Intrusions into the tropical upper troposphere, *Geophys. Res. Lett.*, 27, 3857-3860.

Webster, P., and J. Holton (1982), Cross-equatorial response to middle-latitude forcing in a zonally varying basic state, *J. Atmos. Sci.*, 39, 722-733.

Waters, J. W., et al. (2006), The Earth Observing System Microwave Limb Sounder (EOS MLS) on the Aura satellite," *IEEE Trans. Geosci. Remote Sensing 44*, no. 5.

Yamazaki, K, and M. Chiba (1993), A 3-D global simulation of the advective transport of passive tracers from various northern hemisphere sources, *Tellus*, 45B, 160-178.

Yevich, R., and J. A. Logan (2003), An assessment of biofuel use and burning of

agricultural waste in the developing world, *Global Biogeochem. Cycles*, 17(4), 1095, doi:10.1029/2002GB001952.

Yienger, J. J., M. Galanter, T. A. Holloway, M. J. Phadnis, S. K. Guttikunda, G. R. Carmichael, W. J. Moxim, and H. Levy II (2000), The episodic nature of air pollution transport from Asia to North America, *J. Geophys. Res.*, 105, 26,931-26,945.

Zhang, G. J., and N. A. McFarlane (1995), Sensitivity of climate simulations to the parameterization of cumulus convection in the Canadian climate centre general circulation model, *Atmos. Ocean*, *33*, 407-446.

Figure Captions:

Figure 1a. Time-longitude plot of monthly meridional CO fluxes averaged between 16ºN and 16ºS from MLS at 147 hPa during September 2004-August 2006. Negative values correspond to southward transport.

Figure 1b. Time-longitude plot of monthly meridional CO fluxes averaged between 16ºN and 16ºS from GEOS-Chem simulation at 147 hPa during 2005. The y axis is set from September 2004 to September 2006 for better comparison with Figure 1a.

Figure 1c. Time-longitude plot of monthly meridional CO fluxes averaged between 16ºN and 16ºS from MOPITT at 150 hPa from January 2000 to December 2006.

Figure 2a. Spatial distribution of monthly mean 147 hPa CO mixing ratios (color contours) from MLS (top) and GEOS-Chem (bottom) during January 2005. Also shown are corresponding wind vectors (arrows) from the NCAR/NCEP reanalysis.

Figure 2b. Same as Figure 2b, but for July 2005.

Figure 3a. GEOS-chem simulated monthly Asian fossil fuel CO fluxes at 147 hPa (color contour) during January 2005. Also shown are the corresponding NCEP reanalysis winds (arrows) and GPCP precipitation rates (line contour).

Figure 3b. Same as Figure 3a, but for July 2005.

Figure 4a. Latitude-time cross sections of upper tropospheric CO mixing ratios (color contours) for year 2005 from MLS (147 hPa), MOPITT (150 hPa) and GEOS-Chem (147 hPa) over the tropical Indian Ocean (60°-100°E). CO mixing ratios are 5-day averages. Also shown are corresponding monthly precipitation rates (line contours) from GPCP.

Figure 4b. Same as Figure 4a, but for the tropical Eastern Pacific.

Figure 5a. Latitude-time cross sections of 147 hPa 'tagged' CO tracer (see text for details) mixing ratios for year 2005 from GEOS-Chem over the tropical Indian Ocean .

Figure 5b. Same as Figure 5a, but for the tropical Eastern pacific.

Figure 6a. Pressure-latitude cross-section of GEOS-Chem simulated CO mixing ratios from NH anthropogenic sources over the Eastern Pacific (100ºW-140ºW) during January 2005. Also shown are NCEP reanalysis winds (arrows) with vertical velocity multiplied by 1000 for better illustration.

Figure 6b. Same as Figure 6a, but for the Indian Ocean (60ºE-100ºE) during July 2005.

Figure 7a. Pressure-latitude cross-section of MOPITT CO mixing ratios over the Eastern Pacific (100ºW-140ºW) during January 2005. Also shown are NCEP reanalysis winds (arrows) with vertical velocity multiplied by 1000.

Figure 7b. Same as Figure 7a, but for the Indian Ocean during July 2005.

Figure 8. Correlation between 5-day averaged CO difference between 16ºN and 16ºS versus precipitation over the Indian Ocean during June-September 2005. CO data are from MLS 147 hPa retrieval and MOPITT 150 hPa retrieval.

Figure 9. Sea surface temperature and wind vector anomalies during January-February 2005.

Figure 1a.

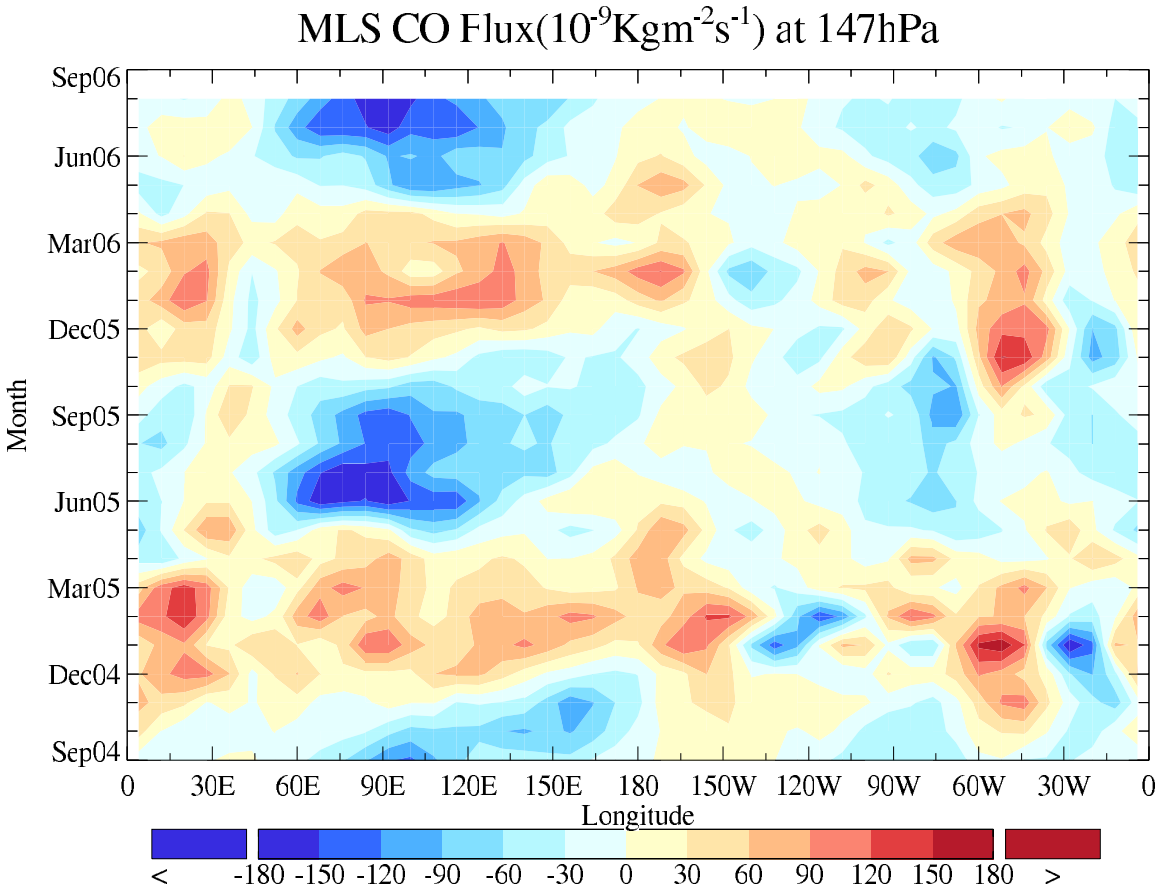

Figure 1a. Time-longitude plot monthly meridional CO fluxes averaged between 16ºN to 16ºS from MLS at 147hPa during September 2004- August 2006. Note that negative values correspond to southward transport.

Figure 1b.

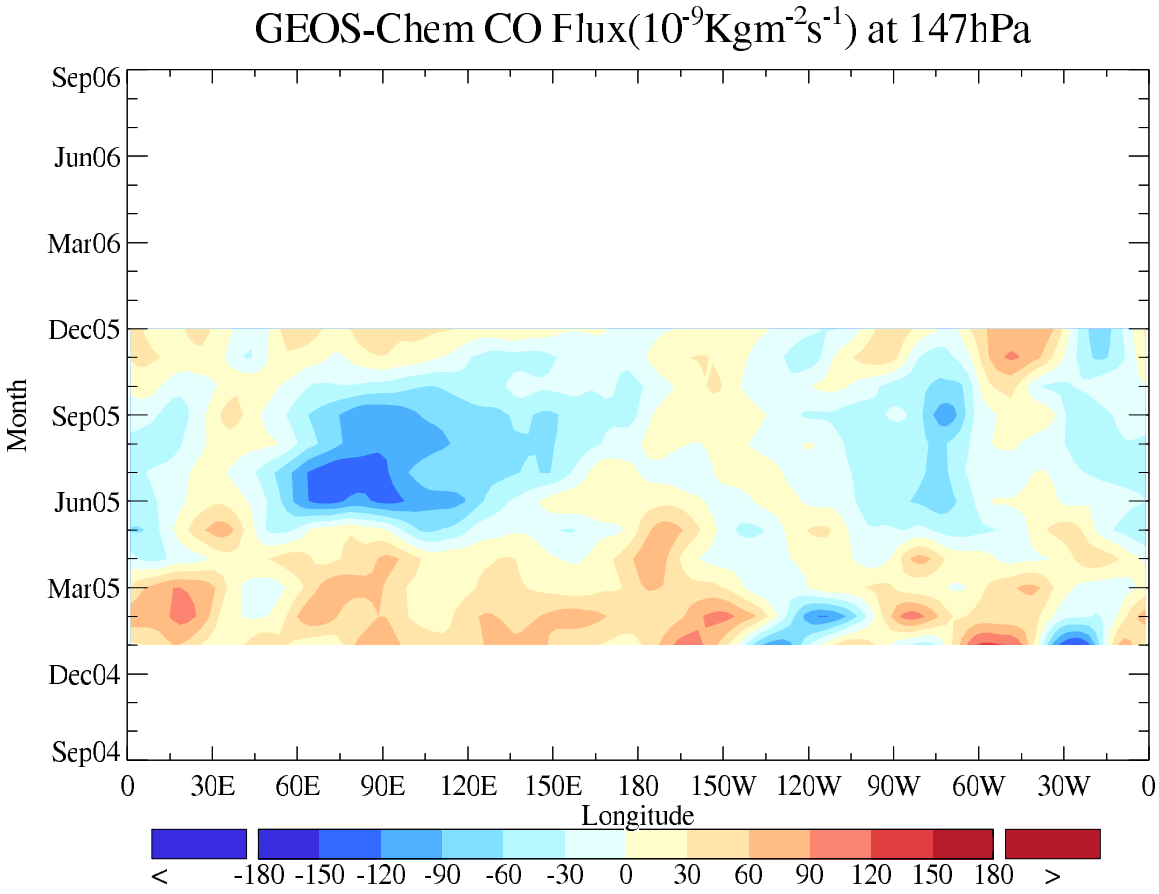

Figure 1b. Time-longitude plot for monthly meridional CO fluxes averaged between 16°N to 16°S from GEOS-Chem simulation at 147hPa during 2005 (y axis is set from Sep04 to Sep06 for comparison with Figure 1a).

Figure 1c.

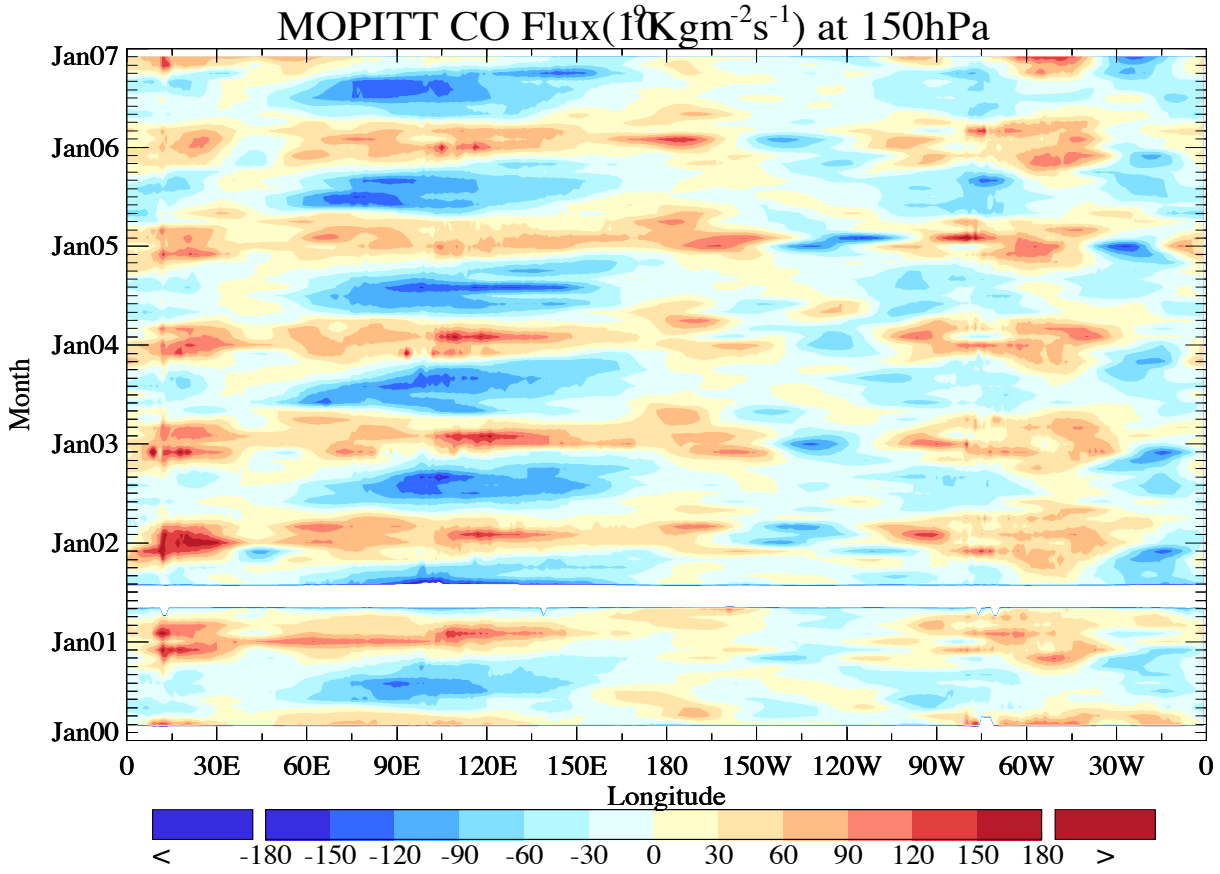

Figure 1c. Time-longitude plot for monthly meridional CO fluxes averaged between 16ºN to 16ºS from MOPITT at 150hPa from January 2000 to December 2006.

Figure 2a.

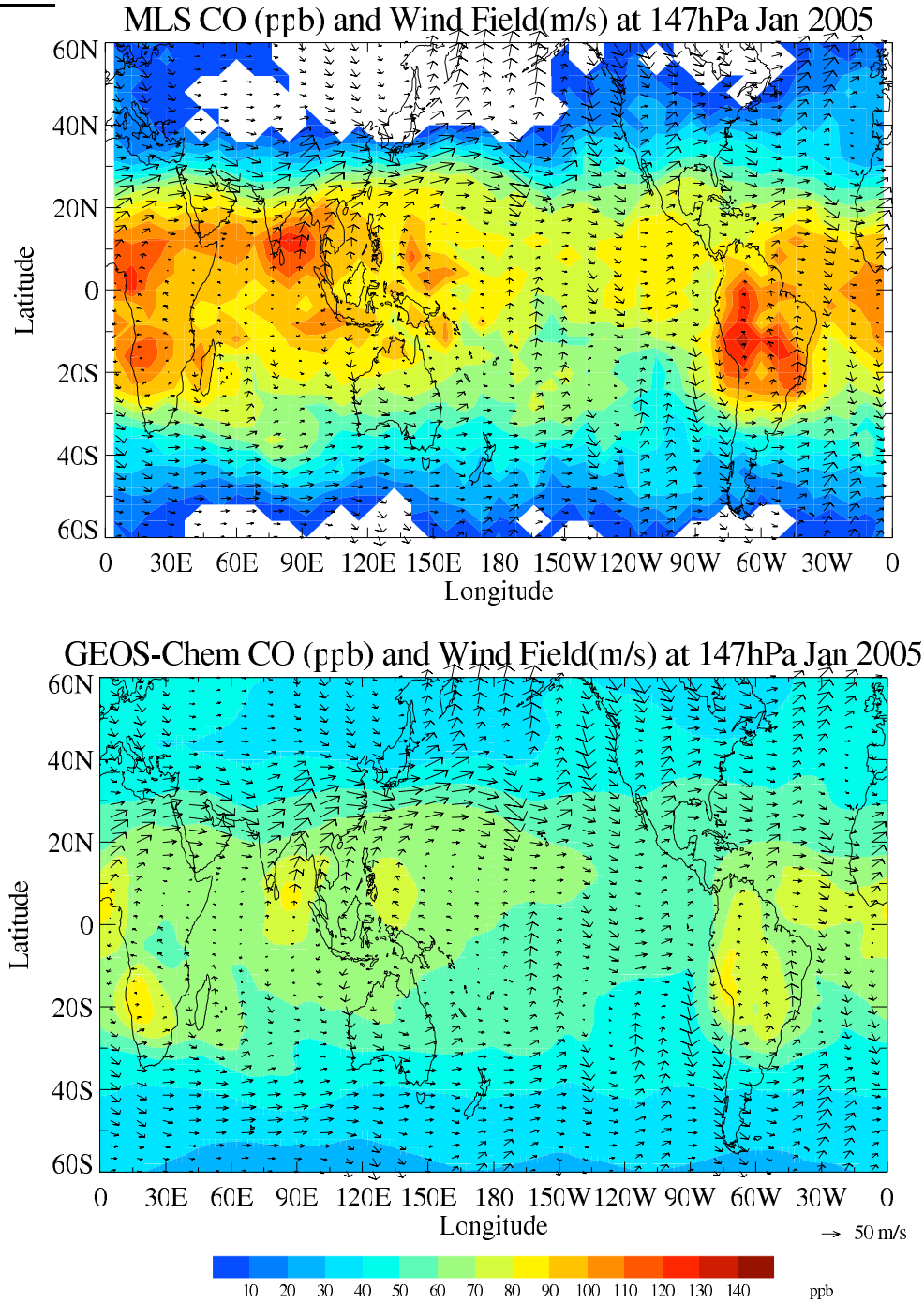

Figure 2a. Spatial distribution of monthly means of 147 hPa CO mixing ratios (color contours) from MLS (top) and GEOS-Chem (bottom) during January 2005. Also shown are corresponding wind vectors (arrows) from NCAR/NCEP reanalysis.

Figure 2b.

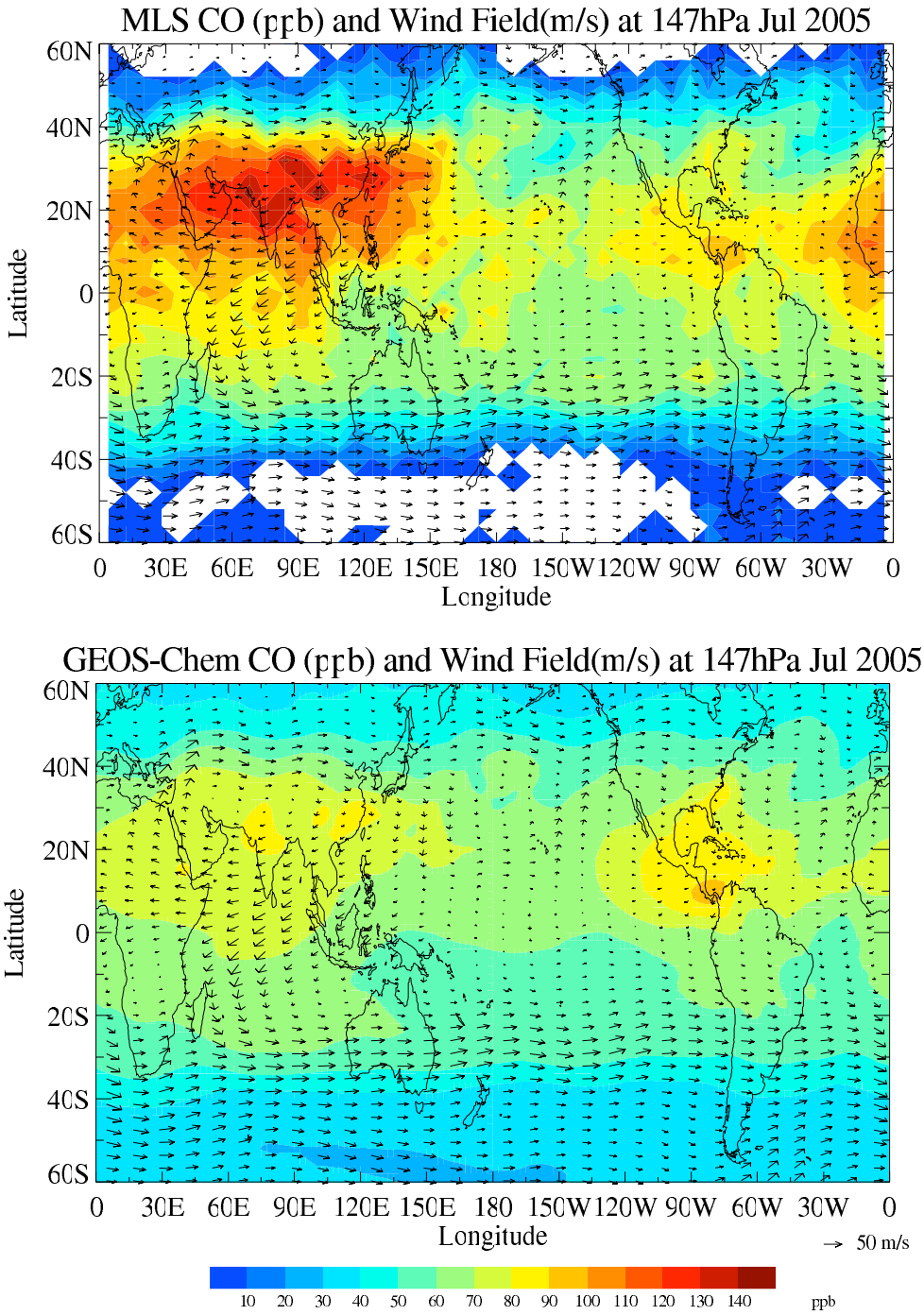

Figure 2b. Same as Figure 2a, but for July 2005.

Figure 3a.

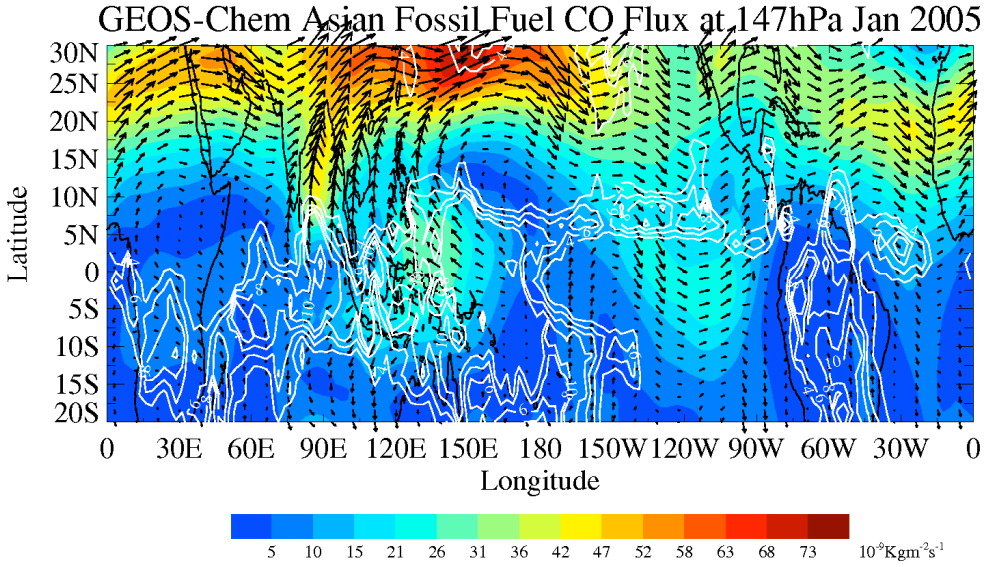

Figure 3a. GEOS-chem simulated monthly Asian fossil fuel CO fluxes at 147 hPa (color contour during January 2005. Also shown are corresponding NCEP reanalysis winds (arrows) and GPCP precipitation (line contour).

Figure 3b.

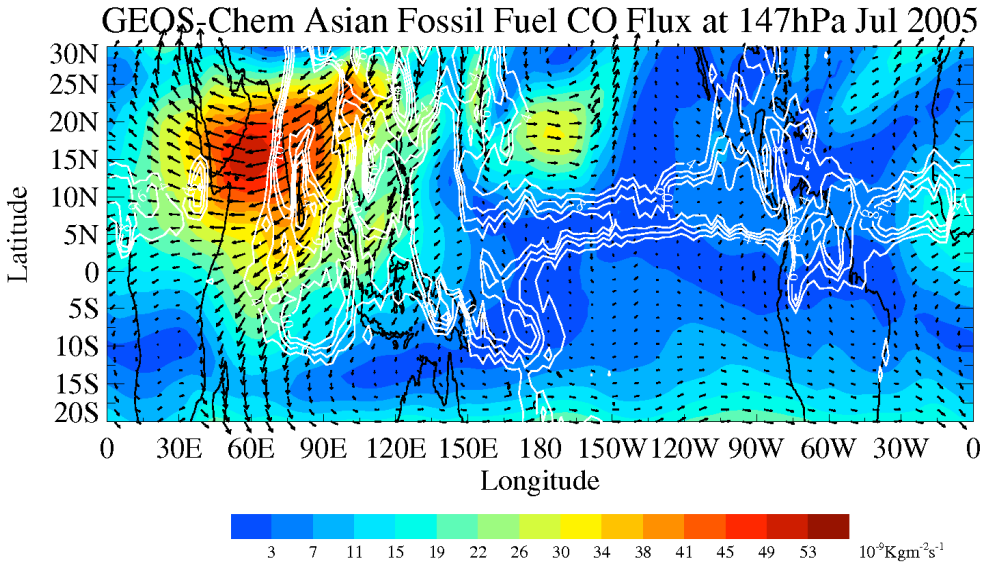

Figure 3b. Same as Figure 3a, but for July 2005.

Figure 4a.

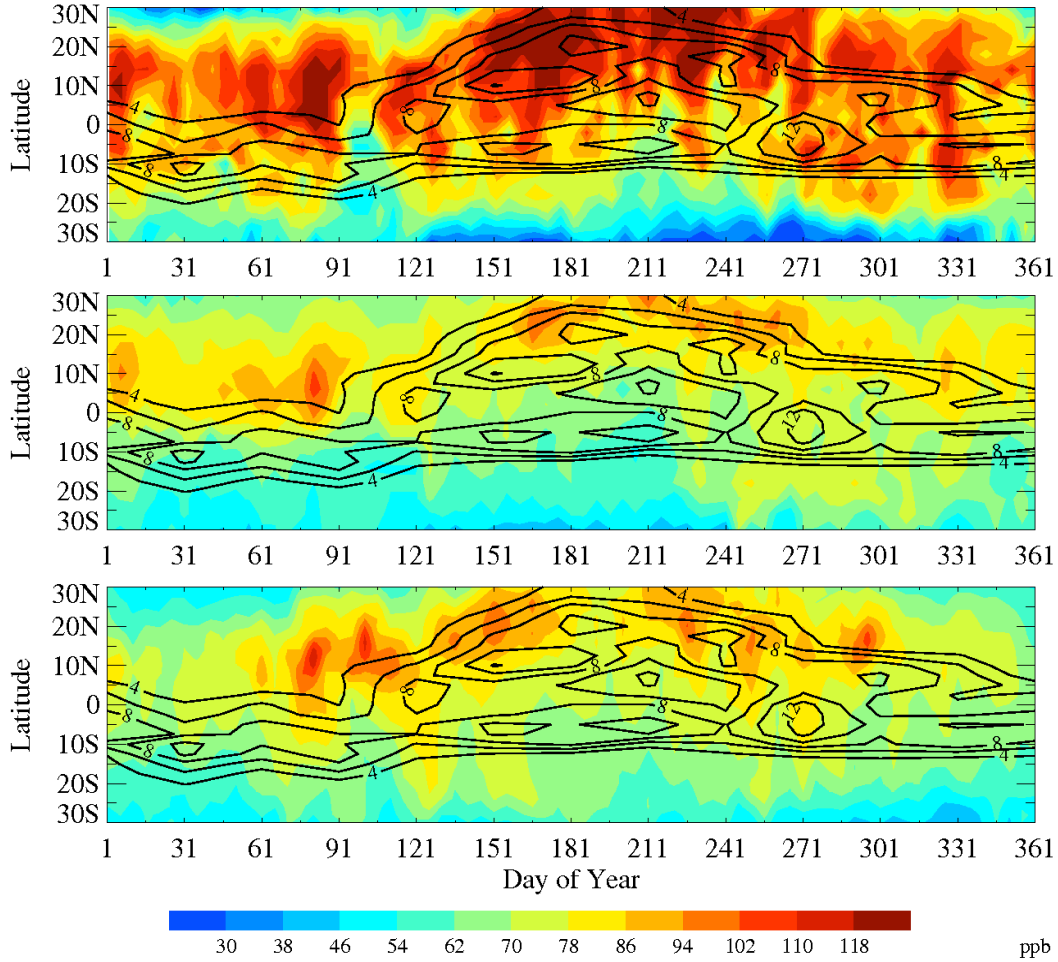

Figure 4a. Latitude-time cross sections of upper tropospheric CO mixing ratios (color contours) for year 2005 from MLS (147hPa), MOPITT(150hPa) and GEOS-Chem(147hPa) over the tropical Indian Ocean (60°-100°E). All the CO mixing ratios area are 5-day averages. Also shown are corresponding monthly precipitation rates (line contours) from GPCP (available at http://precip.gsfc.nasa.gov/index.html).

Figure 4b

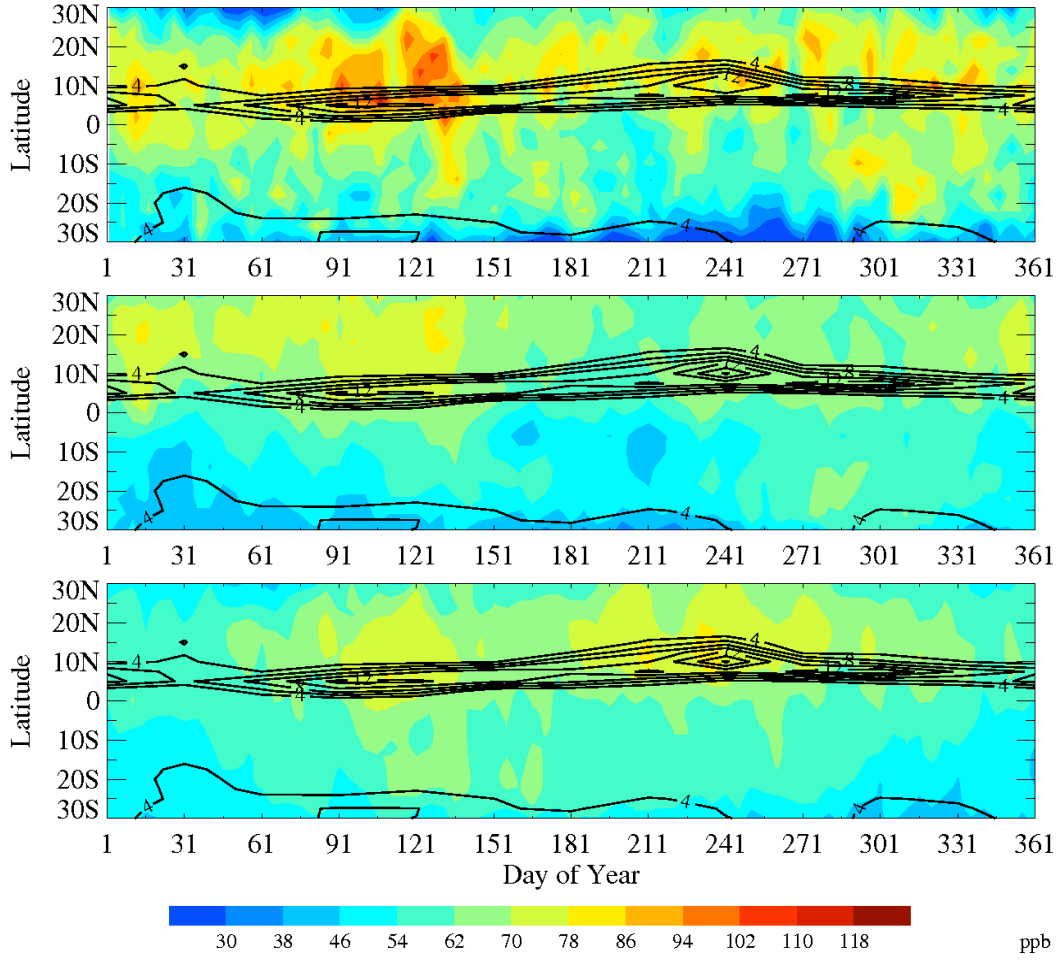

Figure 4b. Same as Figure 4a, but for the tropical Eastern pacific.

Figure 5a.

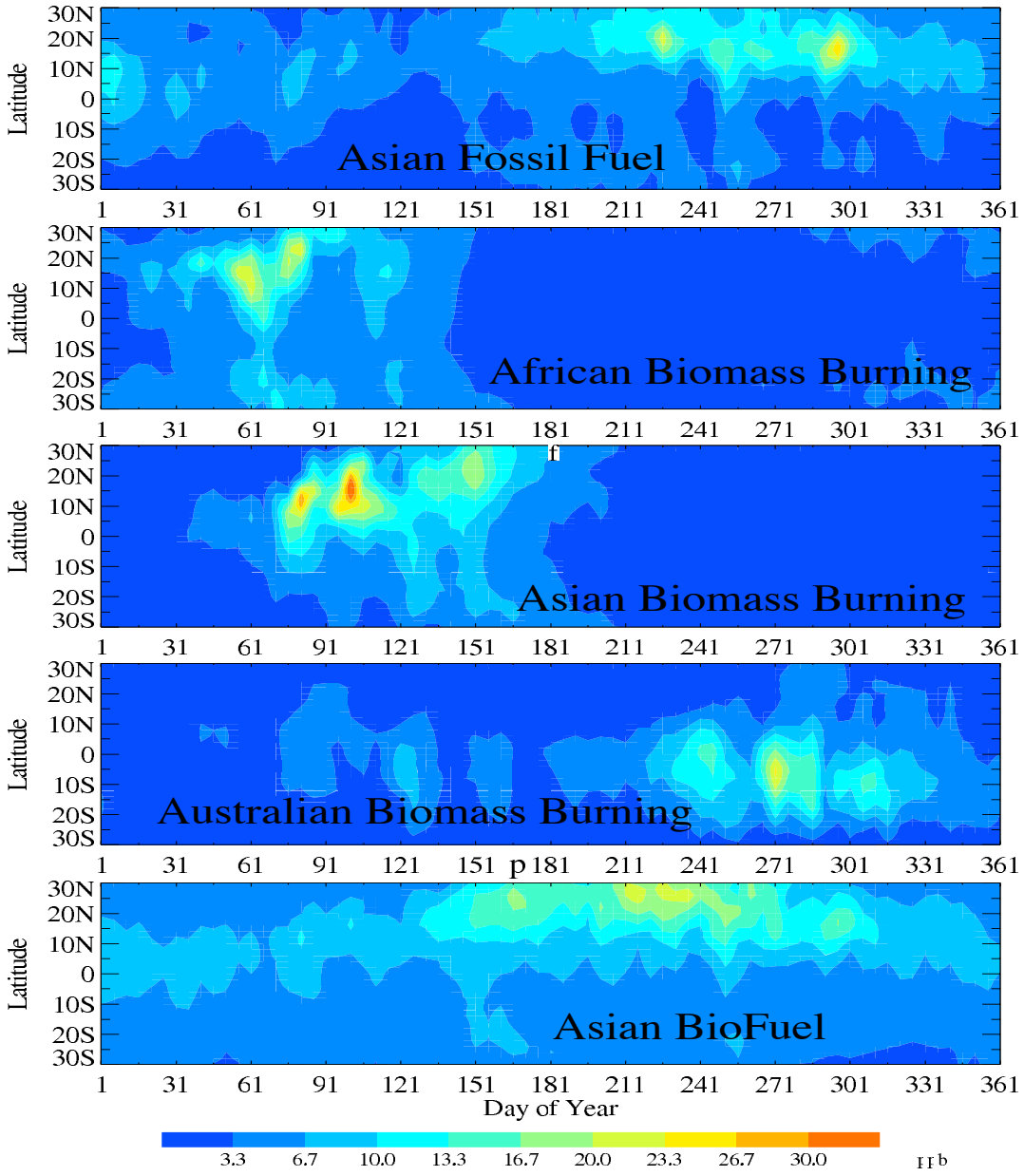

Figure 5a. Latitude-time cross sections of 147 hPa 'tagged' CO tracer (see text for details) mixing ratios for year 2005 from GEOS-Chem over the tropical Indian Ocean .

Figure 5b.

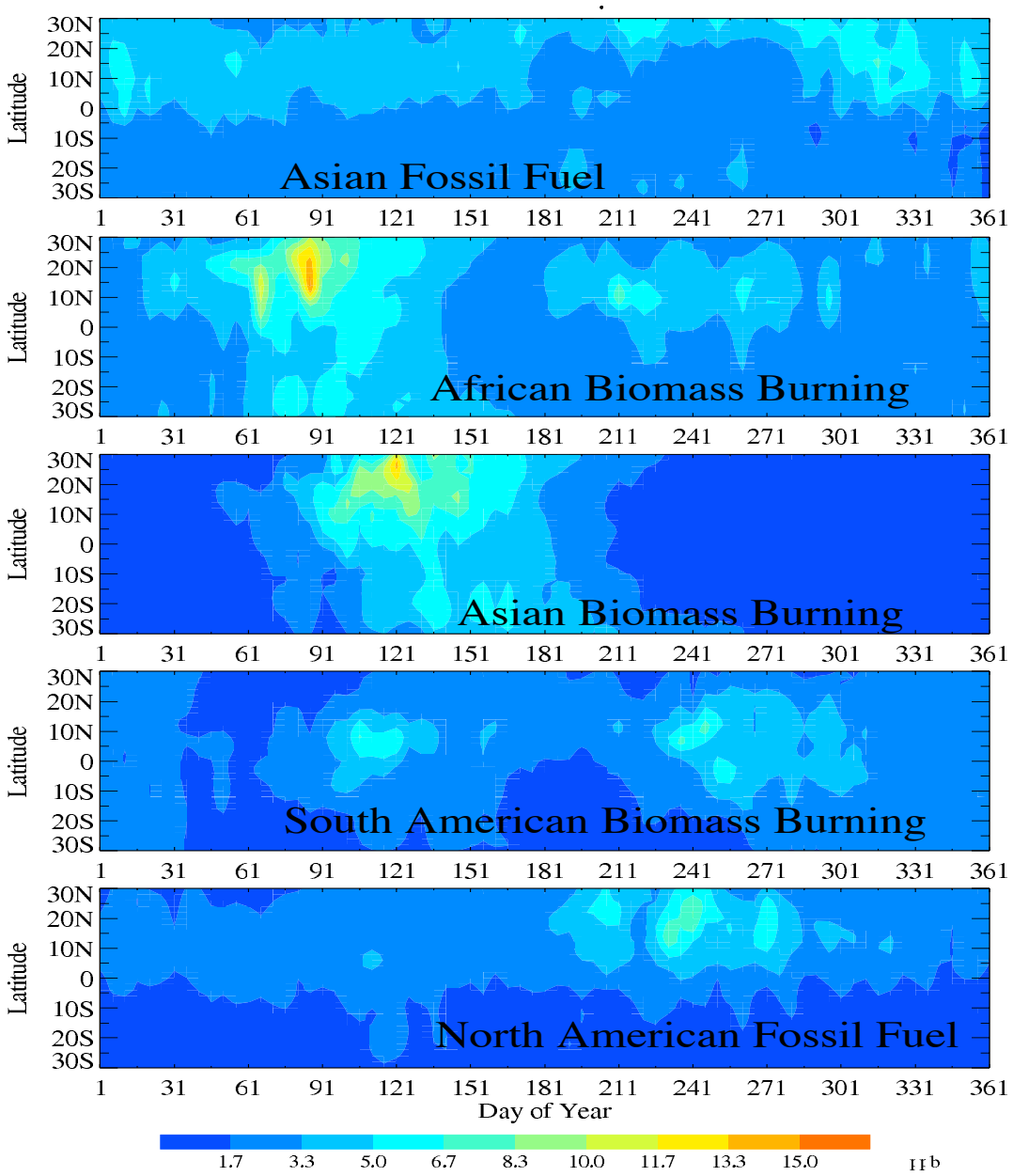

Figure 5b. Same as Figure 5a, but for the tropical Eastern pacific.

Figure 6a.

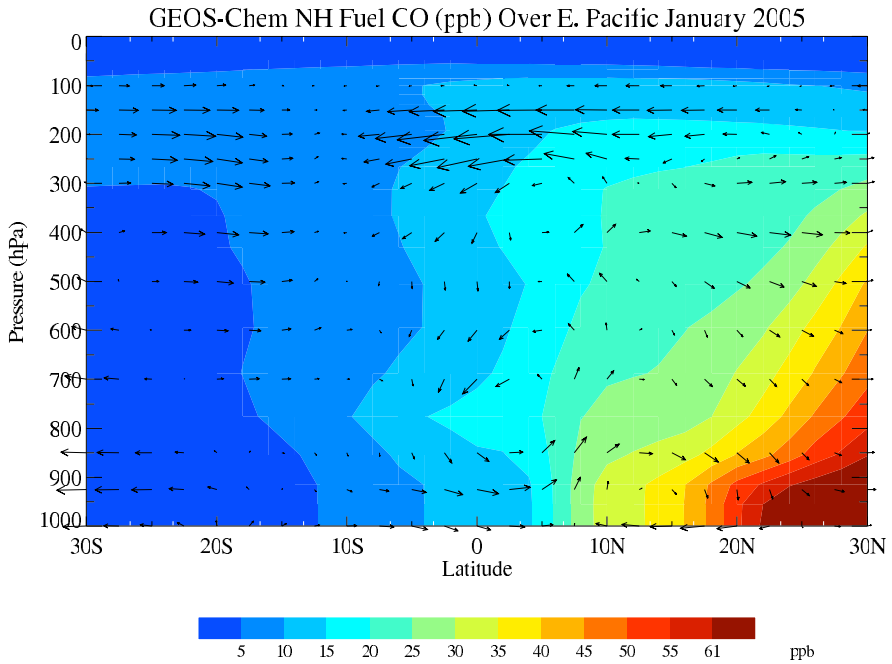

Figure 6a. Pressure-latitude cross-section of GEOS-Chem simulated CO mixing ratios from Northern Hemisphere fuel tracers over the Eastern Pacific (100ºW-140ºW) during January 2005. Also shown are NCEP reanalysis winds (arrows) with vertical velocity multiplied by 1000.

Figure 6b.

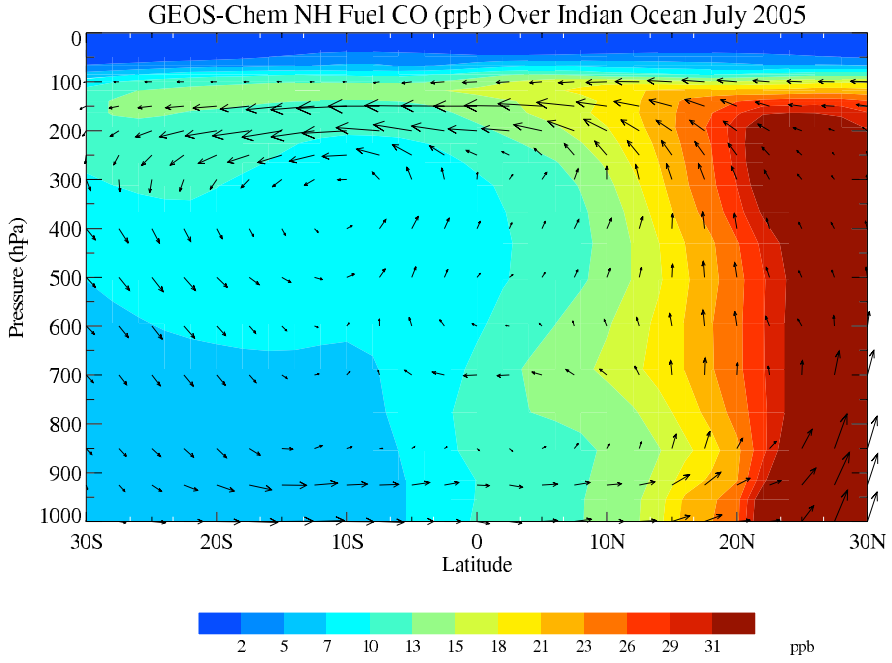

Figure 6b. Same as Figure 6a, but for the Indian Ocean (60ºE-100ºE) during July 2005.

Figure 7a.

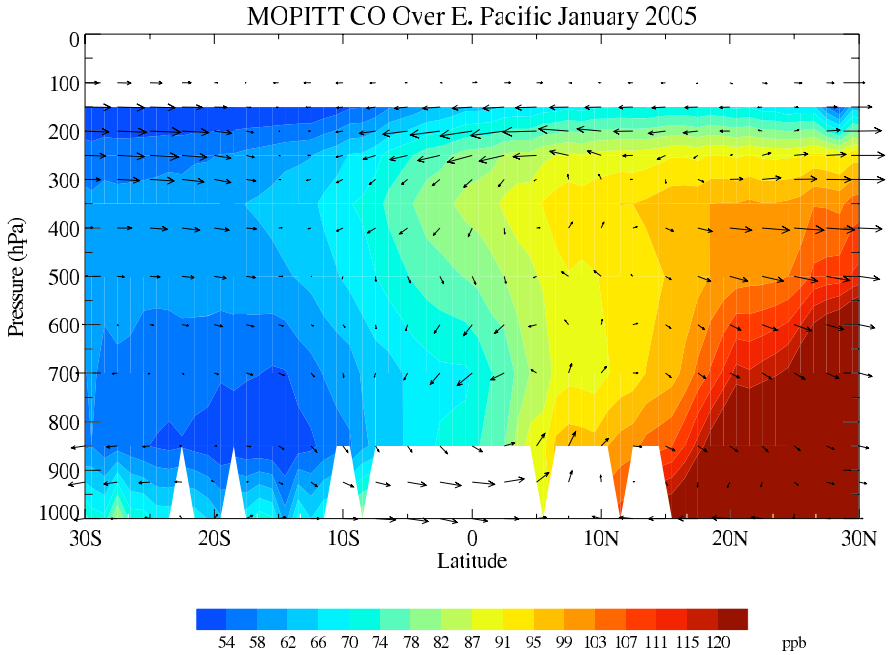

Figure 7a. Pressure-latitude cross-section of MOPITT CO mixing ratios over the Eastern Pacific (100ºW-140ºW) during January 2005. Also shown are NCEP reanalysis winds (arrows) with vertical velocity multiplied by 1000.

Figure 7b.

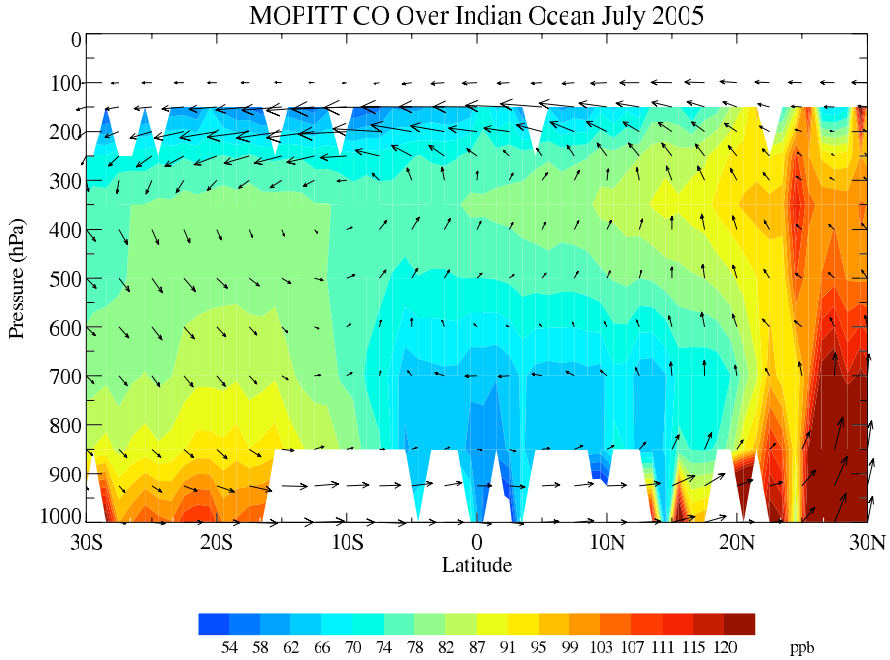

Figure 7b. Same as Figure 7a, but for the Indian Ocean during July 2005.

Figure 8.

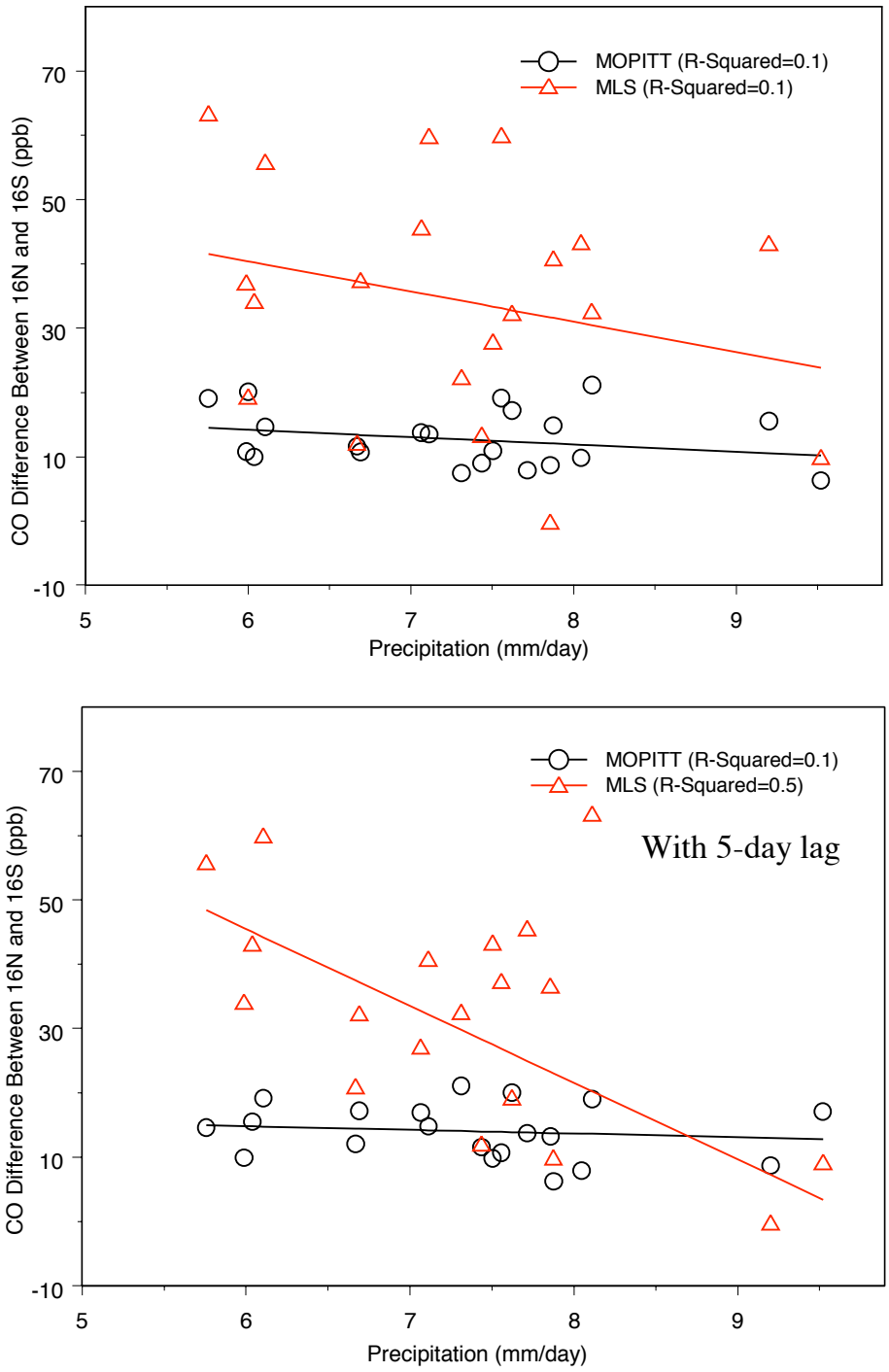

Figure 8. Correlation between 5-day average CO difference between 16ºN and 16ºS vs. precipitation over the Indian Ocean during 2005 summer monsoon months (JJAS). CO data are from MLS 147hPa retrieval and MOPITT 150hPa retrieval.

Figure 9.

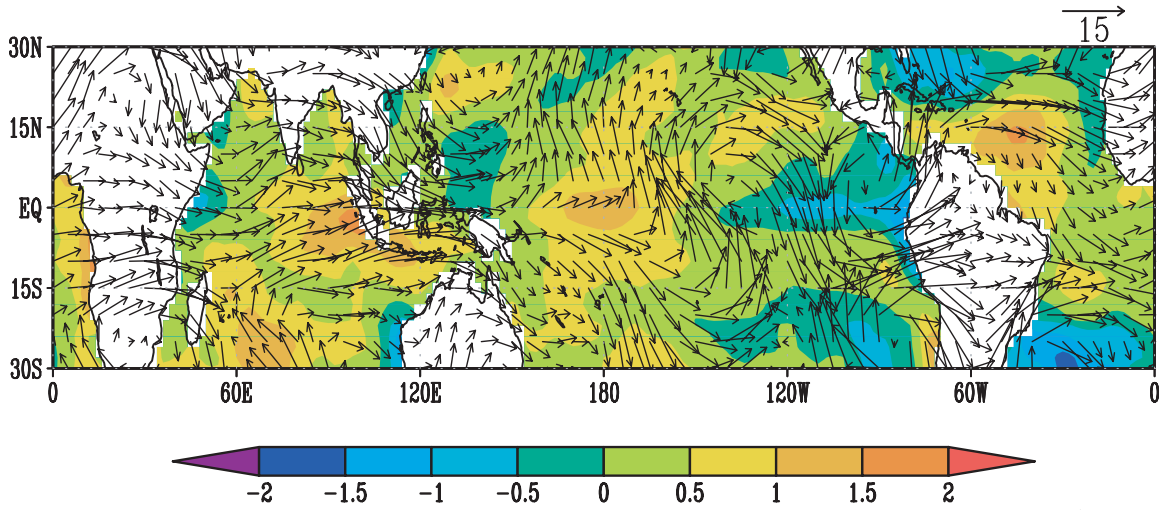

Figure 9: SST (unit: ºC) and wind vector (unit: m/s) anomalies during Jan-Feb 2005.